



Constructing a system for effective utilization of photogenerated electrons and holes: Photocatalytic selective transformation of aromatic alcohols to aromatic aldehydes and hydrogen evolution over $Zn_3In_2S_6$ photocatalysts

Xiangju Ye^a, Yinghao Chen^a, Yahui Wu^b, Xuemei Zhang^a, Xuchun Wang^a, Shifu Chen^{a,b,*}

^a College of Chemistry and Materials Engineering, Anhui Science and Technology University, Bengbu, 233030, PR China

^b Key Lab of Clean Energy and Green Circulation, HuaiBei Normal University, HuaiBei, 235000, PR China



ARTICLE INFO

Keywords:
Photocatalysis
 $Zn_3In_2S_6$
Aromatic alcohol
Aromatic aldehyde
Hydrogen

ABSTRACT

In a reaction system, the simultaneously efficient utilization of photogenerated electrons and holes to realize the photocatalytic selective redox reactions of organics has been a hot topic. In this paper, the $Zn_3In_2S_6$ samples were synthesized via a simple solvothermal method with different solvents, which could make full use of photogenerated electrons and holes to achieve the photocatalytic selective transformation of aromatic alcohols to aromatic aldehydes and hydrogen evolution under mild conditions. The results show that the $Zn_3In_2S_6$ synthesized with water ($Zn_3In_2S_6\text{-W}$) exhibits the highest photocatalytic performance among the selected samples, with which the yields of benzaldehyde and hydrogen reach up to 732 and 708.8 μmol under light irradiation ($\lambda \geq 380\text{ nm}$) for 4 h, respectively. The molar ratios between aldehydes and hydrogen are close to 1: 1. The apparent quantum efficiency is about 6.48% for wavelength $\lambda = 380 \pm 10\text{ nm}$ over $Zn_3In_2S_6\text{-W}$ sample. A possible reaction mechanism for the photocatalytic selective transformation of benzyl alcohol to benzaldehyde and hydrogen evolution under light irradiation is proposed. This work highlights that a reaction system is developed to effectively make use of the photogenerated electrons and holes for selective transformation of aromatic alcohols to aromatic aldehydes and hydrogen evolution over $Zn_3In_2S_6$ photocatalysts under mild conditions.

1. Introduction

Because water and sunlight are abundant, green and environmental-friendly resources, solar-driven hydrogen evolution (SHE) is considered to be an attractive and potential strategy to meet the increasing serious energy and environmental problems [1–3]. Since the previous report about the development of a photoelectrochemical device using Pt-TiO₂ electrode for H₂ evolution from water splitting in 1972, considerable efforts have been devoted to design highly efficient semiconductor photocatalysts for hydrogen evolution [4–7]. Unfortunately, TiO₂ ($E_g = 3.2\text{ eV}$) is only responsive to the UV region of solar spectrum, which greatly restricts its industrial applications. Thus, in the recent years, a range of visible light-response semiconductor photocatalysts, such as C₃N₄, CdS and Cd_xZn_{1-x}S etc. have been widely investigated [8–10]. For example, Wang and his co-workers firstly introduced C₃N₄ as a heterogeneous photocatalyst for the photocatalytic H₂ evolution in the presence of Pt co-catalyst [11]. However, in most cases, the rates of total photocatalytic reactions of water splitting are very low because

the sluggish water oxidation half-reaction does not match well with the reduction side half-reaction [12]. In order to improve the rate of H₂ evolution, the synergistic effect of co-catalysts (such as Pt, phosphorene, MoS₂) and hole scavenger (e.g., methanol, ethanol and lactic acid) is developed [11,13–17]. This can facilitate charge separation and then improve the photocatalytic H₂ evolution, which, however, results in the waste of a large number of photogenerated hole energy.

It is known that the partially oxidation of alcohols to carbonyl compounds is one of the most significant transformations in organic synthesis and has attracted widespread interest [18–22]. The traditional selective oxidation of alcohols to corresponding aldehydes can be realized in the presence of stoichiometric oxygen donors, such as chromate, permanganate, hypochlorite and peroxy acids. However, these are all hazardous, toxic, and produce a number of by-products in the reactions [23–26]. Therefore, it is necessary to develop a new reaction system to realize the above reaction in the environmentally friendly condition. In recent years, photocatalytic selective oxidation of aromatic alcohols to aromatic aldehydes in O₂ atmosphere has been

* Corresponding author at: Key Lab of Clean Energy and Green Circulation, HuaiBei Normal University, HuaiBei, 235000, PR China.
E-mail address: chshifu@chnu.edu.cn (S. Chen).

investigated extensively. In this reaction system, O_2 captures the photogenerated electrons to form superoxide radical, which contributes to the oxidation of alcohols to aldehydes in the presence of photo-generated holes [27–29]. Recently, selective oxidation of aromatic alcohols to aromatic aldehydes and reduction of nitrobenzene to aniline in a reaction system under nitrogen atmosphere has been achieved by our research group. In the reaction system, aromatic alcohols are dehydrogenated into aromatic aldehydes by the photogenerated holes, and nitrobenzene is hydrogenated to aniline by the photogenerated electrons. The photogenerated holes and electrons are effectively used in the reaction system [20,25,30]. Based on the above result, it gives an inspiration that whether it can be realized to develop a new reaction system for efficient utilization of photogenerated electrons and holes for photocatalytic transformation of benzyl alcohol to benzaldehyde and H_2 evolution.

It is known that ternary chalcogenide, $Zn_mIn_2S_{3+m}$ ($m = 1\text{--}5$), has been attracted more and more attention in photocatalytic field [31], such as photocatalytic water splitting [32], degradation of organic pollutants [33,34] and organic transformation [35]. For example, Wang et al. reported that $CdS/ZnIn_2S_4$ heterogeneous structure was synthesized successfully by a solvothermal method and had excellent photo-electron-chemical performance [36]. Our group has demonstrated that the oxidation of aromatic alcohols to aromatic aldehydes is achieved by the synergistic effect of $Zn_3In_2S_6$ and ZnO [26]. It has been reported that the band gap of $Zn_3In_2S_6$ is $2.5 \sim 2.8$ eV, which can be introduced as a visible-light response photocatalyst. The valence band (VB) and conduction band (CB) positions are about $2.1 \sim 2.4$ and -0.3 to -0.5 eV, respectively, suggesting that it is a potential material for the photocatalytic transformation of aromatic alcohols to corresponding aldehydes and H_2 evolution.

Herein, $Zn_3In_2S_6$ samples were synthesized by a simple solvothermal method with different solvents and were characterized by a series of techniques. The resulted samples are capable of effective utilization of photogenerated electrons and holes for photocatalytic transformation of aromatic alcohols to aromatic aldehydes and H_2 evolution under mild conditions. The $Zn_3In_2S_6$ -W shows the best photocatalytic activity among the studied samples, and the apparent quantum efficiency of $Zn_3In_2S_6$ -W sample with $\lambda = 380 \pm 10$ nm is 6.48%. The photogenerated electrons and holes play important roles in the photocatalytic reaction process. A possible reaction mechanism for the photocatalytic selective transformation of benzyl alcohol to benzaldehyde and hydrogen evolution under light irradiation is proposed. This paper not only provides a new strategy for effective use of photogenerated electrons and holes, but also expands a new photocatalytic reaction system, such as nitrogen fixation and CO_2 reduction.

2. Experimental

2.1. Materials

Zinc sulfate heptahydrate ($ZnSO_4 \cdot 7H_2O$), indium chloride tetrahydrate ($InCl_3 \cdot 4H_2O$), thiacetamide (CH_3CSNH_2), benzyl alcohol, p-fluorobenzyl alcohol, p-methoxybenzyl alcohol, o-, m- and p- methylbenzyl alcohol were purchased from Aladdin Regent (Shanghai, China). All chemicals used in the experiments were analytical pure grade and were used without further purification. Deionized water was used throughout this study.

2.2. Preparation of photocatalysts

$Zn_3In_2S_6$ was synthesized by a simple solvothermal method with different solvents. Typically, 3 mmol $ZnSO_4 \cdot 7H_2O$, 2 mmol $InCl_3 \cdot 4H_2O$ and 6 mmol CH_3CSNH_2 were dissolved in 70 mL deionized water by stirring for 30 min. Then, the obtained homogeneous solution was transferred into a 100 mL Teflon-lined autoclave and was heated at 160°C for 12 h. After cooling to room temperature, the precipitate was

collected by centrifugation and washed thoroughly with deionized water several times. The final product was dried in a vacuum oven at 80 °C for 8 h. The as-obtained sample was denoted as $Zn_3In_2S_6$ -W. The $Zn_3In_2S_6$ synthesized with other different solvents were synthesized by a similar method as that for the preparation of $Zn_3In_2S_6$ -W except for the use of different solvents. The $Zn_3In_2S_6$ synthesized with ethanol, methanol, ethylene glycol were denoted as $Zn_3In_2S_6$ -E, $Zn_3In_2S_6$ -M, $Zn_3In_2S_6$ -EG, respectively. For comparison, other photocatalysts, such as $Cd_{0.5}Zn_{0.5}S$, $ZnIn_2S_4$, CdS and In_2S_3 were also synthesized by a similar method as that for the preparation of $Zn_3In_2S_6$ -W.

2.3. Characterization

The crystallographic structures of $Zn_3In_2S_6$ samples were analyzed by powder X-ray diffraction (XRD) using a Bruker D8 advance X-ray diffractometer with $Cu K\alpha$ radiation ($\lambda = 0.154056$ nm) and a scanning speed of 3°/min. The crystallite size of the samples can be calculated by X-ray line broadening analysis according to the Scherrer's formula. The elemental analysis was carried out on an inductively coupled plasma mass spectrometry (ICP-MS, PerkinElmer, ELAN9000). The X-ray photoelectron spectroscopy (XPS) was measured on a Thermo Scientific ESCA Lab250 spectrometer with an $Al K\alpha$ X-ray beam. The binding energies were corrected with reference to the C 1 s peak of the surface adventitious carbon at 284.6 eV. The optical properties was characterized by UV-vis diffuse reflectance spectroscopy (UV-vis DRS) using a UV-vis spectrophotometer (Shimadzu UV-2550). The morphologies and microstructures of the photocatalysts were studied by scanning electron microscopy (SEM, JEOL7800 F). Transmission electron microscopy (TEM) and high-resolution transmission electron microscopy (HRTEM) images were performed with a FEI-G2 transmission electron microscope with an accelerating voltage of 200 kV. The Brunauer-Emmett-Teller (BET, ASAP2020) was used to determine the specific surface area and pore size distribution of the samples. Photoluminescence (PL) properties of the samples were analyzed using a fluorescence spectrometer (RF530, Shimadzu Scientific Instruments Inc., Japan). The time-resolved photoluminescence (TRPL) spectra were measured by a PicoHarp300 (PicoQuant) instrument. Electron paramagnetic resonance (EPR) spectra were obtained on an EPR Spectrometer (A300, Bruker, Germany) using 5,5-dimethyl-1-pyrroline-N-oxide (DMPO) as the spin-trap reagent.

2.4. (Photo)electrochemical tests

(Photo)electrochemical experiments were performed on a CHI-660 electrochemical work station (Chenhua Instruments Co., China) using a conventional three-electrode. A Pt wire and $Ag/AgCl$ electrode were used as counter electrode and reference electrode, respectively. The $Zn_3In_2S_6$ /FTO electrode was used as the working electrode (50 mm × 50 mm). The preparation of the working electrode is as follows: the sample powder (5 mg) was dispersed in 0.5 mL of deionized water by sonication to obtain a slurry. The slurry was spread onto the fluoride tin oxide (FTO) glass, whose side part had been previously protected using scotch tape. After air drying, the working electrode was further dried at 80°C for 2 h to improve adhesion. A copper wire was connected to the side of the working electrode using conductive tape. Uncoated parts of the electrode were isolated with epoxy resin. A quartz cell filled with 0.1 M Na_2SO_4 or 0.1 M KCl electrolyte containing 0.1 M $K_3[Fe(CN)_6]$ / $K_4[Fe(CN)_6]$ was used as the reaction system. In the photocurrent experiments, the light source was a 300 W Xe arc lamp (CEL-HXF300E7, Beijing China Education Au-light Co., Ltd.) with a UV-CUT filter ($\lambda \geq 420$ nm).

2.5. Evaluation of photocatalytic activity

Photocatalytic selective transformation of aromatic alcohols to aromatic aldehydes and H_2 evolution was carried out in a Pyrex top-

irradiation reaction vessel connected to a glass closed gas circulation system (CEL-SPH2N, Beijing China Education Au-light Co., Ltd., China), and the reaction temperature was controlled at about 10 °C by using a recirculation cooling system. Typically, 0.1 g catalyst was dispersed in 100 mL benzyl alcohol. Then, the reactant solution was degassed by using a mechanical pump and stirred for 30 min in the dark to remove the air completely. The produced H₂ in the reaction process was measured by an online gas chromatograph (GC7920, Beijing China Education Au-light Co., Ltd., China). After the reaction, the reacted solution was centrifuged for three times to remove the photocatalyst powder and then was detected by using a gas chromatograph (GC 2014, Shimadzu). A 300 W Xe arc lamp (CEL-HXF300E7, Beijing China Education Au-light Co., Ltd.) system equipped with a UV-cut filter ($\lambda > 380$ nm) was used as a light source.

The yield and selectivity of aromatic aldehydes were defined as follows:

$$\text{Yield (\%)} = \left(\frac{\text{C}_{\text{aldehyde}}}{\text{C}_0} \right) \times 100 \quad (1)$$

$$\text{Selectivity (\%)} = \left[\frac{\text{C}_{\text{aldehyde}} - (\text{C}_0 - \text{C}_{\text{alcohol}})}{\text{C}_0} \right] \times 100 \quad (2)$$

where C₀ was the initial concentration of aromatic alcohols; C_{alcohol} and C_{aldehyde} were the concentrations of residual aromatic alcohols and the corresponding aromatic aldehydes at a certain time after the photocatalytic reaction, respectively.

According to the reaction mechanism, one molecule of aromatic aldehydes would be produced by consuming two photogenerated holes, releasing two protons. Subsequently, one H₂ molecule would be formed by consuming of two electrons and two protons. Thus, the utilization rate (R_U) of photogenerated electrons relative to holes could be calculated by the following equation:

$$R_U = \left(\frac{\text{Numbers of evolved H}_2}{\text{Numbers of aromatic aldehydes}} \right) \times 100\% \quad (3)$$

3. Results and discussion

3.1. Characterization of photocatalysts

XRD is used to determine the crystal phase and crystallographic structure of the as-synthesized samples. As shown in Fig. 1, it is clear that the Zn₃In₂S₆ samples synthesized with different solvents all exhibit similar XRD patterns. The peaks located at 21.5°, 27.6°, 28.8°, 47.6° and 56.3° could be indexed as (005), (100), (102), (110) and (203) facets, respectively, suggesting that the XRD peaks of Zn₃In₂S₆ can be assigned to a hexagonal phase. No other diffraction peaks of impurity phase, such as zinc sulfide or indium sulfide are observed in XRD patterns, indicating the phase purity of the as-prepared Zn₃In₂S₆ samples. Meanwhile, it is worth noting that the Zn₃In₂S₆ synthesized with water

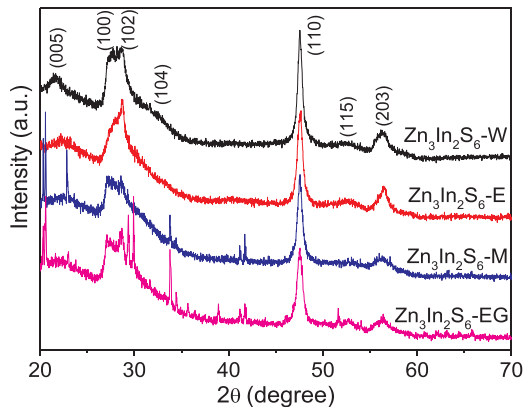


Fig. 1. XRD patterns of Zn₃In₂S₆ samples synthesized with different solvents.

(Zn₃In₂S₆-W) exhibits a relatively good crystallinity, which may be conducive to improving its photocatalytic performance. The particle sizes of the Zn₃In₂S₆ samples can be estimated according to the Scherrer's formula. The average crystallite sizes of Zn₃In₂S₆-W, Zn₃In₂S₆-E, Zn₃In₂S₆-M and Zn₃In₂S₆-EG samples are about 12.2, 14.7, 13.5 and 16.2 nm, respectively. The constitution of the sample was also proved by inductively coupled plasma-mass spectrometry (ICP-MS) measurements. The result shows that the molar ratio of Zn:In:S in the sample is 3.3:2.1:6, which is close to the stoichiometric composition.

The surface chemical composition and element valence states of Zn₃In₂S₆-W are examined by X-ray photoelectron spectroscopy (XPS). The results are shown in Fig. 2. The survey spectrum in Fig. 2a shows that the elements of In, Zn, S, C and O are all detected in Zn₃In₂S₆-W sample. Among these, the peaks of C and O mainly originate from the absorbed gaseous molecules and the graphite conductive adhesive, respectively. The high-resolution spectra of Zn, In and S are shown in Fig. 2(b-d). It is clear that two characteristic peaks at 1022.0 and 1045.1 eV are in good agreement with Zn 2p_{2/3} and Zn 2p_{1/2}, respectively, reflecting that the Zn species exists as Zn²⁺. The high resolution In 3d spectrum is composed of two individual peaks of In 3d_{5/2} and In 3d_{1/2} at 443.8 and 451.3 eV, respectively, which is assigned to In³⁺. The S 2p spectrum indicates that the peak can be divided into two peaks. One is located at ca. 161.3 eV (S 2p_{2/3}) and the other is at ca. 162.4 eV (S 2p_{1/2}), implying that the valence state of S is the -2. The results are consistent with the as-prepared sample and the previous reports [32,34,37], which indicates that the Zn₃In₂S₆-W sample is successfully synthesized by a solvothermal method.

Fig. 3 shows the microscopic structure and morphology information of as-prepared Zn₃In₂S₆ samples. It can be seen that the Zn₃In₂S₆ samples synthesized with different solvents have different morphologies. It is clear that the microsphere structure of Zn₃In₂S₆-W sample with smooth surfaces is made of cross-linked nanosheets, and the size of the microspheres is ca. 1–3 μm (Fig. 3a). The Zn₃In₂S₆-M is made of microspheres and irregular blocks, and the size is about 1–3 μm (Fig. 3b). The Zn₃In₂S₆-E sample aggregates together, and the morphology turns to be very irregular (Fig. 3c). And the Zn₃In₂S₆-EG sample also shows a microspheres structure with a diameter in the range of 0.5–2 μm (Fig. 3d). The above result will result in the differences of the BET specific surface area among the as-obtained samples, which further affects their photocatalytic performance. Meanwhile, TEM and HRTEM analyses were applied to further investigate the microstructure of Zn₃In₂S₆-W samples (Fig. 4). The TEM images of the as-prepared Zn₃In₂S₆-W sample in Fig. 4(a–c) demonstrate that the sample is composed of relatively uniform sphere-like Zn₃In₂S₆ architectures with slight aggregation, and each sphere consists of numerous two-dimensional petals, which is in agreement with SEM results (Fig. 3a). The high-resolution TEM (HRTEM) image of Zn₃In₂S₆-W sample is presented in Fig. 4d. It is obvious that a lattice fringe spacing is 0.32 nm, corresponding to the (102) crystal plane of Zn₃In₂S₆, which is consistent with the XRD pattern. Moreover, to further clarify the composition profile of Zn₃In₂S₆-W, TEM-mapping analysis is carried out. It shows that the In, Zn and S elements are uniformly distributed in the sample (Fig. 4e).

The optical properties of the Zn₃In₂S₆ samples synthesized with different solvents are examined by UV-vis diffuse reflectance spectroscopy (UV-vis DRS). As shown in Fig. 5, the Zn₃In₂S₆ samples have strong photoabsorption ability and the absorption edge of the Zn₃In₂S₆ samples synthesized with different solvents are approximately 500 nm, implying that they can function as potential visible light-driven photocatalysts. Moreover, the band gap energy of the semiconductor can be estimated according to the following formula [20,21,23,25]:

$$a\lambda h = A(h\nu - E_g)^{n/2}$$

where a, h, ν, E_g and A correspond to the absorption coefficient, Planck constant, optical frequency, band gap energy, and proportionality

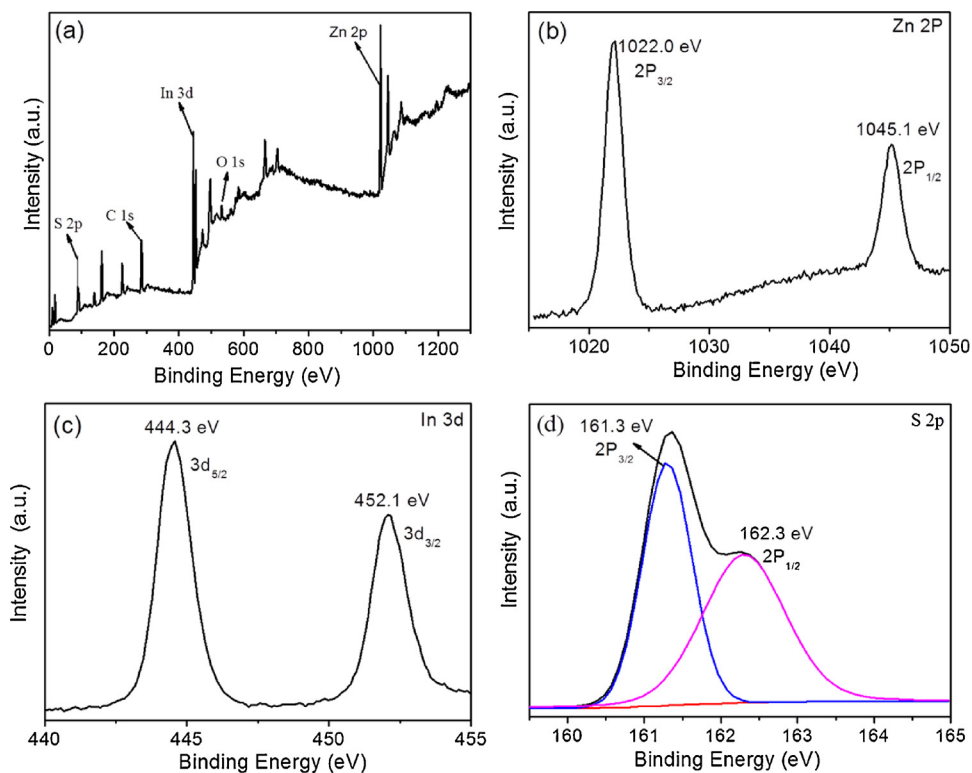


Fig. 2. XPS spectra of the as-prepared $\text{Zn}_3\text{In}_2\text{S}_6$ survey spectrum(a) and high-resolution spectra of Zn 2 P(b), In 3d (c), and S 2p(d).

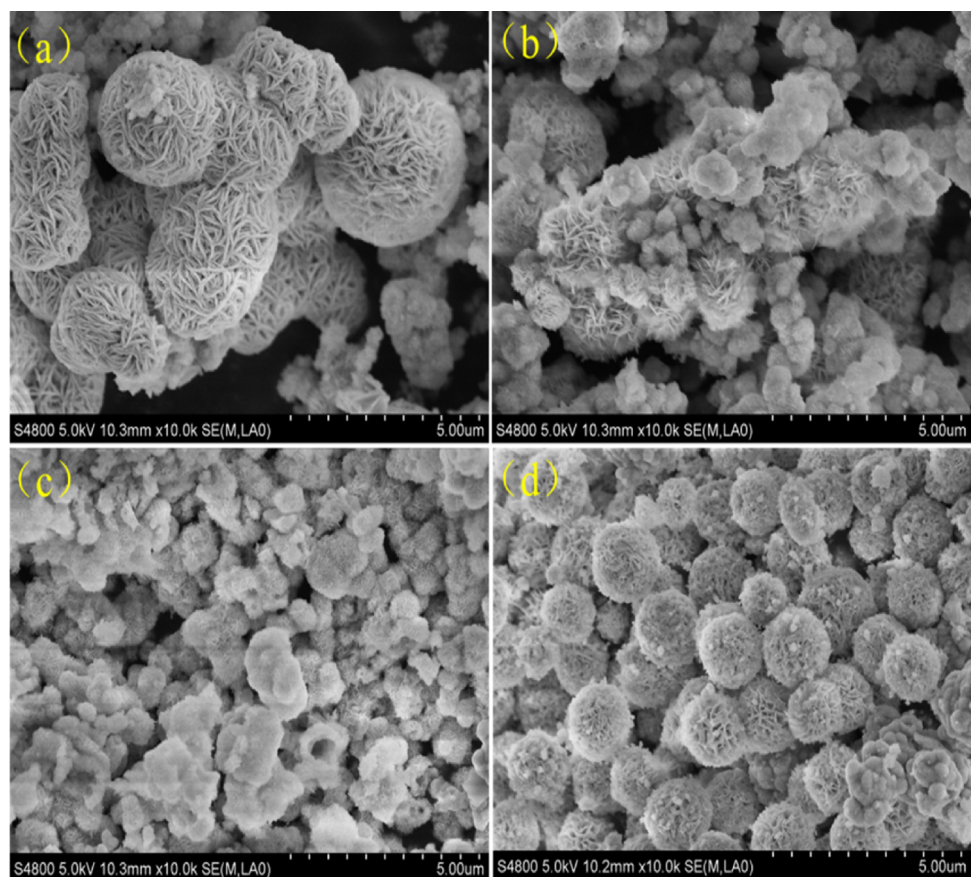


Fig. 3. SEM images of $\text{Zn}_3\text{In}_2\text{S}_6$ -W(a), $\text{Zn}_3\text{In}_2\text{S}_6$ -E(b), $\text{Zn}_3\text{In}_2\text{S}_6$ -M(c) and $\text{Zn}_3\text{In}_2\text{S}_6$ -EG(d).

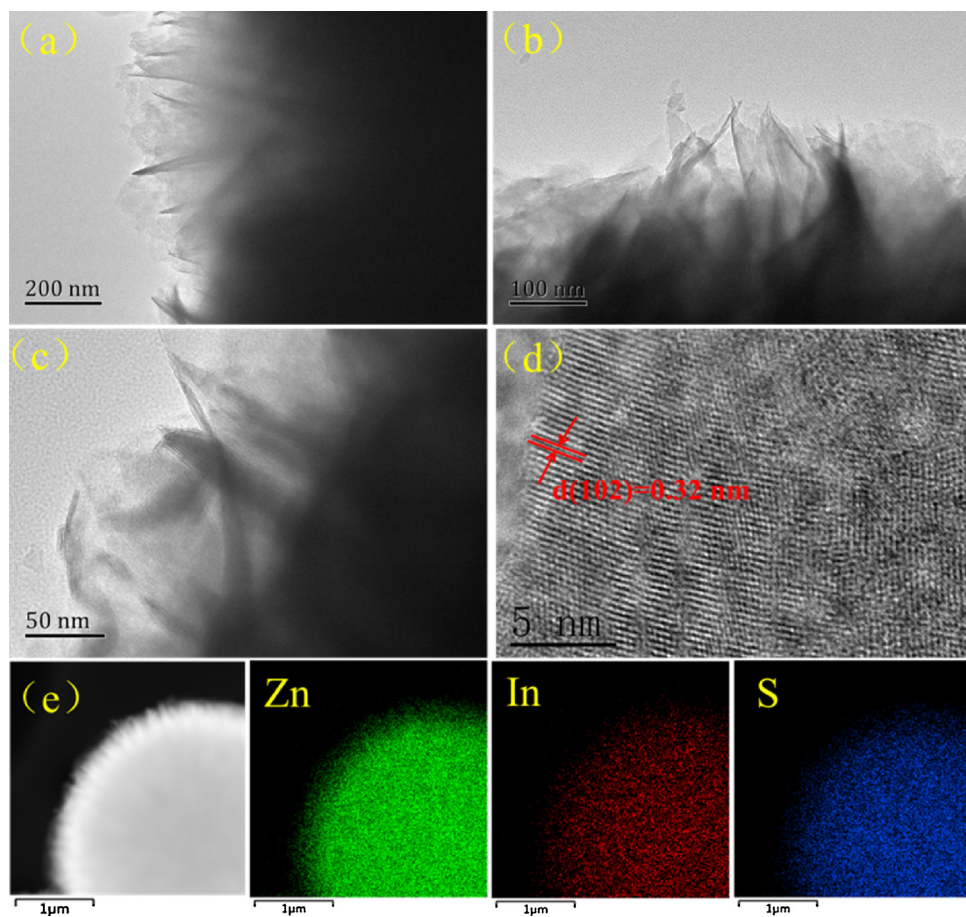


Fig. 4. TEM(a–c), HRTEM (d) and TEM-mapping images (e) of $\text{Zn}_3\text{In}_2\text{S}_6$ -W sample.

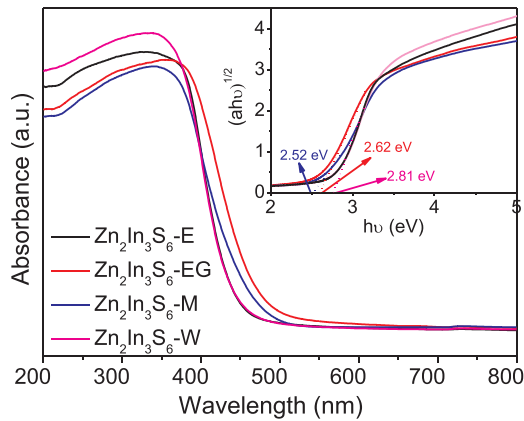


Fig. 5. UV-vis DRS spectra and $(ahv)^{1/2}$ versus $h\nu$ curve (inset) of $\text{Zn}_3\text{In}_2\text{S}_6$ samples.

coefficient, respectively, and n stands for the type of the transition in a semiconductors ($n = 1$ for direct transition, and $n = 4$ for indirect transition). In previous report, we know that the $\text{Zn}_3\text{In}_2\text{S}_6$ sample is indirect transition semiconductor [26]. Thus, the band gap energy (E_g) of $\text{Zn}_3\text{In}_2\text{S}_6$ -W, $\text{Zn}_3\text{In}_2\text{S}_6$ -E, $\text{Zn}_3\text{In}_2\text{S}_6$ -M, and $\text{Zn}_3\text{In}_2\text{S}_6$ -EG samples are 2.81, 2.81, 2.62 and 2.52 eV, respectively.

Nitrogen adsorption-desorption analysis is performed to investigate the BET specific surface area and pore-size distribution of the samples. As shown in Fig. 6, the adsorption-desorption isotherms of the samples are IV type adsorption isotherms according to the IUPAC classification, reflecting that the resulted $\text{Zn}_3\text{In}_2\text{S}_6$ samples belong to the mesoporous structure [20,29]. From the SEM and TEM images, it

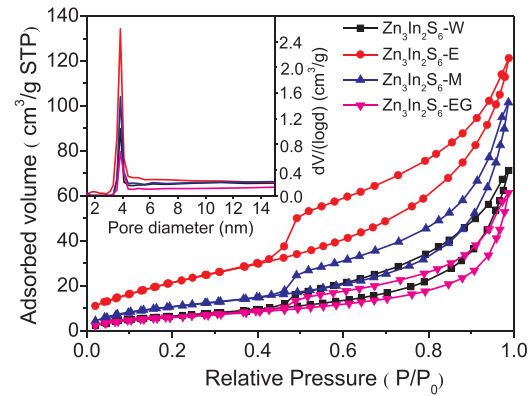


Fig. 6. Nitrogen adsorption-desorption isotherms of $\text{Zn}_3\text{In}_2\text{S}_6$ samples and the corresponding pore-size distribution curves.

can be found that the mesoporous structure of the $\text{Zn}_3\text{In}_2\text{S}_6$ -W sample originates from the loose stacking of the cross-linked nanosheets and the assembled microspheres. Additionally, the $\text{Zn}_3\text{In}_2\text{S}_6$ samples synthesized with different solvents have the similar pore size distribution. The average pore diameters of $\text{Zn}_3\text{In}_2\text{S}_6$ -W, $\text{Zn}_3\text{In}_2\text{S}_6$ -E, $\text{Zn}_3\text{In}_2\text{S}_6$ -M and $\text{Zn}_3\text{In}_2\text{S}_6$ -EG are approximately 3.830, 3.837, 3.836 and 3.822 nm, respectively. The BET specific surface area of $\text{Zn}_3\text{In}_2\text{S}_6$ -W, $\text{Zn}_3\text{In}_2\text{S}_6$ -E, $\text{Zn}_3\text{In}_2\text{S}_6$ -M and $\text{Zn}_3\text{In}_2\text{S}_6$ -EG are 55.02, 128.76, 76.42 and $42.30 \text{ m}^2 \text{ g}^{-1}$, respectively. It can be observed that there are distinct differences in the BET specific surface area of the as-prepared samples. From the following activity results, we can deduce that the photocatalytic activity of the sample is not directly related to its specific surface area.

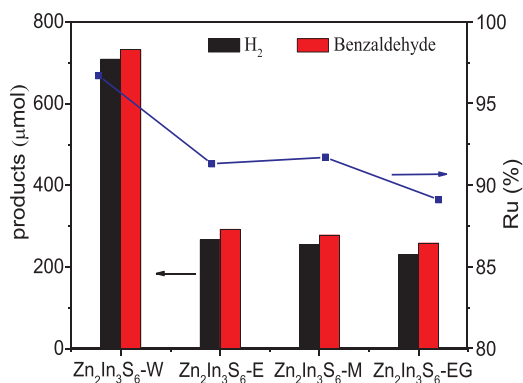


Fig. 7. Photocatalytic transformation of benzyl alcohol to benzaldehyde and H_2 evolution over $\text{Zn}_3\text{In}_2\text{S}_6$ samples synthesized with different solvents under light illumination for 4 h.

3.2. Evaluation of photocatalytic activity

The photocatalytic performance of the as-prepared $\text{Zn}_3\text{In}_2\text{S}_6$ samples is evaluated by a dual-function photocatalytic system under light irradiation ($\lambda > 380 \text{ nm}$), in which benzyl alcohol is selectively oxidized to benzaldehyde by the photogenerated holes, and the released protons are reduced to hydrogen by the photogenerated electrons. The photocatalytic performance of the $\text{Zn}_3\text{In}_2\text{S}_6$ synthesized with different solvents is shown in Fig. 7. It can be found that under light illumination for 4 h, the production amounts of benzaldehyde are 732, 292.3, 278.3 and 258.5 μmol for $\text{Zn}_3\text{In}_2\text{S}_6\text{-W}$, $\text{Zn}_3\text{In}_2\text{S}_6\text{-E}$, $\text{Zn}_3\text{In}_2\text{S}_6\text{-M}$ and $\text{Zn}_3\text{In}_2\text{S}_6\text{-EG}$ photocatalysts, respectively, and the evolution amounts of H_2 for $\text{Zn}_3\text{In}_2\text{S}_6\text{-W}$, $\text{Zn}_3\text{In}_2\text{S}_6\text{-E}$, $\text{Zn}_3\text{In}_2\text{S}_6\text{-M}$ and $\text{Zn}_3\text{In}_2\text{S}_6\text{-EG}$ photocatalyst are 708.8, 266.9, 255.3 and 230.2 μmol , respectively. It is clear that the $\text{Zn}_3\text{In}_2\text{S}_6$ synthesized with water ($\text{Zn}_3\text{In}_2\text{S}_6\text{-W}$) is an excellent photocatalyst for photocatalytic transformation of benzyl alcohol to benzaldehyde and hydrogen evolution among the screened samples. Additionally, the Ru (utilization rate) values of $\text{Zn}_3\text{In}_2\text{S}_6$ samples are also shown in Fig. 7. It can be seen that the Ru values of $\text{Zn}_3\text{In}_2\text{S}_6\text{-W}$, $\text{Zn}_3\text{In}_2\text{S}_6\text{-E}$, $\text{Zn}_3\text{In}_2\text{S}_6\text{-M}$ and $\text{Zn}_3\text{In}_2\text{S}_6\text{-EG}$ photocatalysts are 96.8, 91.3, 91.7 and 89.1%, respectively, implying that $\text{Zn}_3\text{In}_2\text{S}_6\text{-W}$ has the best utilization rate in this reaction system among the $\text{Zn}_3\text{In}_2\text{S}_6$ samples. On the basis of the above experiment results and analysis, it is demonstrated that the yields of benzaldehyde are close to those of hydrogen evolution, and the difference of the yields for benzaldehyde and hydrogen evolution is mainly attributed to the diffusion of the abstracted hydrogen protons from VB to CB of the photocatalyst surface. Therefore, $\text{Zn}_3\text{In}_2\text{S}_6\text{-W}$ will be taken as the model photocatalyst in the following experiments.

Fig. 8 displays the dependence of the photocatalytic activity on the amount of photocatalyst. It can be observed that the benzaldehyde production and H_2 evolution increase with the increase of the amount of $\text{Zn}_3\text{In}_2\text{S}_6$ photocatalyst up to 0.10 g. However, when the amount of photocatalyst is higher than 0.10, the production amounts decrease slightly. The optimized amount of $\text{Zn}_3\text{In}_2\text{S}_6$ in this system is about 0.10 g, with which the yield of benzaldehyde and H_2 for $\text{Zn}_3\text{In}_2\text{S}_6\text{-W}$ photocatalyst are 732 and 708.8 μmol under light irradiation ($\lambda > 380 \text{ nm}$) for 4 h, respectively. This phenomenon can be explained in terms of availability of active sites on the catalyst surface and the penetration of light into the suspension, which have been reported on other fields, such as the photocatalytic transformation of organic compounds and degradation of dyes [22,38,39].

To evaluate the stability of $\text{Zn}_3\text{In}_2\text{S}_6\text{-W}$ sample for the photocatalytic transformation of benzyl alcohol to corresponding aldehyde and H_2 evolution, the reaction system was carried out under a prolonged light illumination ($\lambda \geq 380 \text{ nm}$) for 12 h. As displayed in Fig. 9, the yield of H_2 evolution increases continuously during the given time ($t \leq 12 \text{ h}$), which indicates that it basically forms a linear relationship

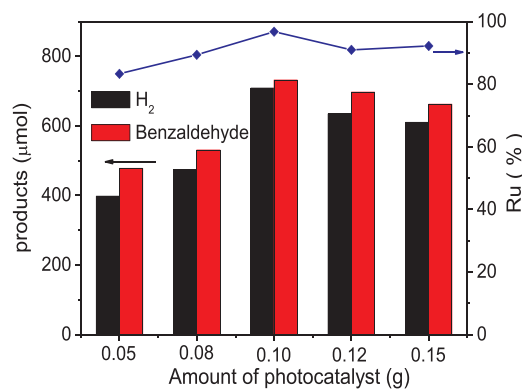


Fig. 8. Photocatalytic oxidation of benzyl alcohol to benzaldehyde and hydrogen evolution with different amount of $\text{Zn}_3\text{In}_2\text{S}_6\text{-W}$ sample under irradiation for 4 h.

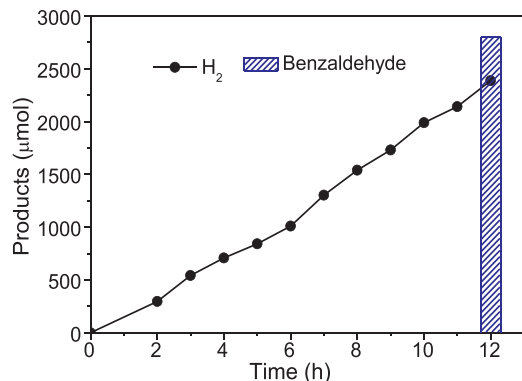


Fig. 9. Time-dependent photocatalytic transformation of benzyl alcohol to benzaldehyde and H_2 evolution over $\text{Zn}_3\text{In}_2\text{S}_6\text{-W}$ sample.

between the amount of H_2 and irradiation time. Furthermore, the yield of benzaldehyde under irradiation for 12 h is 2803.7 μmol , which is close to that of the H_2 evolution (2387.1 μmol). Additionally, the crystal structure of the $\text{Zn}_3\text{In}_2\text{S}_6\text{-W}$ photocatalyst before and after the photocatalytic reaction examined by XRD shows no obvious change (Fig. S1). Hence, it is reasonably considered that $\text{Zn}_3\text{In}_2\text{S}_6\text{-W}$ is a chemically stable photocatalyst for the photocatalytic transformation of benzyl alcohol to benzaldehyde and H_2 evolution under mild conditions.

The apparent quantum efficiency (AQE) of H_2 evolution by $\text{Zn}_3\text{In}_2\text{S}_6\text{-W}$ sample using the incident light wavelength λ_o as a function was measured (summarized in Table 1). Herein, we take $\lambda_o = 400 \text{ nm}$ as an example. The catalyst solution is irradiated by a 300 W Xe lamp with a $400 \pm 10 \text{ nm}$ band-pass filter for 4 h. The average light density is *ca.* $3.43 \text{ mW}\cdot\text{cm}^{-2}$ and the irradiation area is 45.34 cm^2 . Thus, the number of the incident photons (N) is 4.5×10^{21} estimated by the Eq. (4). Meanwhile, the corresponding amounts of H_2 evolution from photocatalytic dehydrogenation of benzyl alcohol are shown in Fig. 10. Therefore, the AQE calculated by the Eq. (5) is 5.46%. The trend of H_2 production matches with the optical absorption of the photocatalyst,

Table 1

The AQE of $\text{Zn}_3\text{In}_2\text{S}_6\text{-W}$ photocatalyst based on the H_2 evolution with different band-pass wavelengths.

Range (nm)	AQE (%)
380 ± 10	6.48
400 ± 10	5.46
420 ± 10	4.02
450 ± 10	1.03

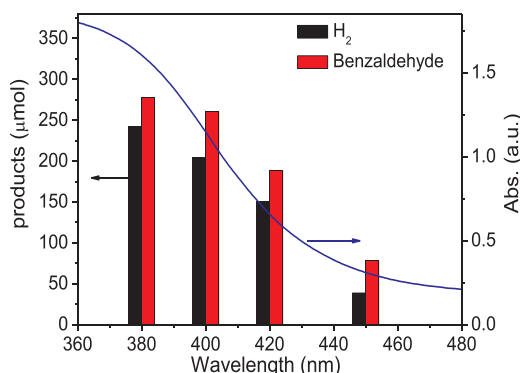


Fig. 10. Relationship between the light wavelength and the yields of benzaldehyde and H₂ over Zn₃In₂S₆-W sample under light illumination for 4 h.

suggesting the reaction indeed proceeds *via* photoabsorption by the photocatalyst. The amount of benzaldehyde in the reaction system is also shown in Fig. 10. It is obvious that the mole ratio between benzaldehyde and hydrogen under light illumination for 4 h is close to 1: 1.

$$\begin{aligned} N &= \frac{E\lambda}{hc} = \frac{3.43 \times 10^{-3} \times 45.34 \times 3600 \times 4 \times 400 \times 10^{-9}}{6.626 \times 10^{-34} \times 3 \times 10^8} \\ &= 4.5 \times 10^{21} \end{aligned} \quad (4)$$

$$\begin{aligned} QE &= \frac{2 \times \text{number of electrons involved in the reaction}}{\text{number of incident photons}} \\ &= \frac{2 \times 6.02 \times 10^{23} \times 204.0 \times 10^{-6}}{4.5 \times 10^{21}} = 5.46\% \end{aligned} \quad (5)$$

To learn more about the wide applicability of Zn₃In₂S₆-W sample, the photocatalytic selective transformation of aromatic alcohols to corresponding aldehydes and H₂ evolution was performed. Herein, P-fluorobenzyl alcohol, p-methylbenzyl alcohol and p-methoxybenzyl alcohol are selected to evaluate the photocatalytic performance of Zn₃In₂S₆-W sample. As shown in Fig. 11, it is clear that the photocatalytic transformation of aromatic alcohols with different substituents to aromatic aldehydes and H₂ can all be realized, but the photocatalytic activity is very different. For example, the yields of benzaldehyde and H₂ are 732 and 708.8 μmol, the yields of p-methoxybenzaldehyde and H₂ are 735.1 and 684.4 μmol, the yields of p-fluorobenzaldehyde and H₂ are 385.9 and 352.4 μmol, and the yields of p-methylbenzaldehyde and H₂ are 427.3 and 373 μmol under light irradiation for 4 h. The result indicates that the electronegativity of the substituents on the phenyl ring did not have a clear effect on the photocatalytic performance, which implies that there is no obvious electronic effect in this reaction [33]. Meanwhile, the o-, m- and p-methoxy-substituted benzyl

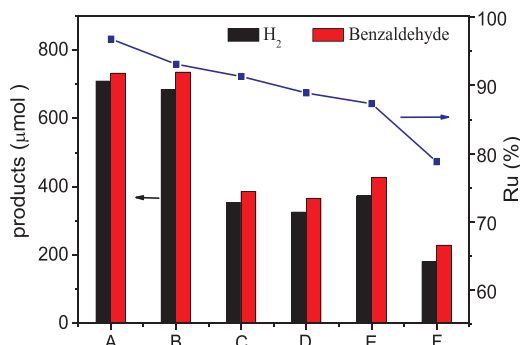


Fig. 11. Photocatalytic transformation of different aromatic alcohols to corresponding aldehydes and H₂ evolution over Zn₃In₂S₆ under light irradiation for 4 h. A: benzyl alcohol, B: p-methoxybenzyl alcohol, C: P-fluorobenzyl alcohol, D: m-methoxybenzyl alcohol, E: p-methylbenzyl alcohol, F: o-methoxybenzyl alcohol.

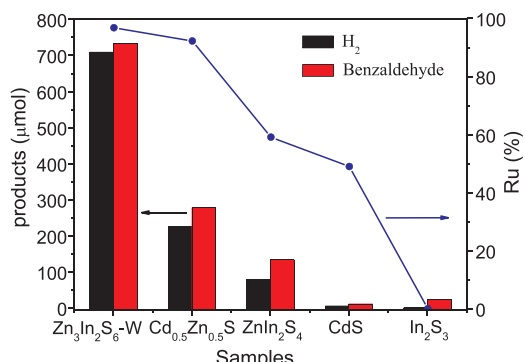


Fig. 12. Photocatalytic oxidation of benzyl alcohol to benzaldehyde and H₂ evolution using different photocatalysts under light irradiation for 4 h.

alcohol as substrates were also investigated (Fig. 11). The result reveals that the amounts of H₂ evolution under light irradiation for 4 h are 180.1, 325.4 and 684.4 μmol, respectively. The activity sequence is as follows: o-methoxybenzyl alcohol < m-methoxybenzyl alcohol < p-methoxybenzyl alcohol. It suggests that the steric hindrance of the substituent has an influence on the photoactivity of selective transformation of aromatic alcohols to aromatic aldehydes and H₂ evolution [33]. Meanwhile, we also calculate the R_U of the products, which are 96.8, 93.1, 91.3, 88.9, 87.3 and 78.8% for benzyl alcohol, p-methoxybenzyl alcohol, P-fluorobenzyl alcohol, m-methoxybenzyl alcohol, p-methylbenzyl alcohol and o-methoxybenzyl alcohol, respectively. It shows that the yield ratios of aldehydes and hydrogen are close to 1: 1 except o-methoxybenzyl alcohol.

To verify the superiority of the as-obtained catalyst, the photocatalytic tests for the selective photocatalytic transformation of benzyl alcohol to benzaldehyde and H₂ evolution using different photocatalysts were also carried out under the same reaction conditions. From Fig. 12, it is obvious that the Zn₃In₂S₆-W sample exhibits the best photocatalytic performance for photocatalytic dehydrogenation of benzyl alcohol to benzaldehyde and H₂ evolution. For example, the yields of the benzaldehyde and H₂ evolution are 732 and 708.8 μmol for Zn₃In₂S₆-W sample, 225.7 and 277.4 μmol for Cd_{0.5}Zn_{0.5}S sample, 78.76 and 133.3 μmol for ZnIn₂S₄ sample, 5.3 and 10.8 μmol for CdS sample, and 0 and 23.2 μmol for In₂S₃ sample under light irradiation for 4 h, respectively. In addition, the corresponding Ru values are 96.8, 92.2, 59.1, 49 and 0, respectively. The results demonstrate that, among the screened samples, Zn₃In₂S₆-W is an optimal photocatalyst for the photocatalytic dehydrogenation of benzyl alcohol to benzaldehyde and H₂ evolution in this reaction system.

In order to explain why Zn₃In₂S₆-W sample exhibits excellent photocatalytic performance, a series of photoelectrochemical experiments, including photocurrent response, electrochemical impedance spectroscopy and Mott-Schottky plots, were carried out. Fig. 13a shows the Photocurrent-Time curves of Zn₃In₂S₆ samples. It can be found that Zn₃In₂S₆-W sample exhibits the largest photocurrent density among the samples. It is generally accepted that the photogenerated hole-electron pairs are produced by the visible-light excitation of the catalyst. Then the photogenerated holes are captured by the holes scavenger in the electrolyte, and the photocurrent is formed by the directional migration of the photogenerated electrons. Thus, it can be concluded that the Zn₃In₂S₆-W sample can produce more photogenerated hole-electron pairs and prolong the lifetime of photogenerated carriers. Meanwhile, the electrochemical impedance spectroscopy (EIS) is implemented to further study the separation and transfer efficiency of the photogenerated carriers. The experiments are conducted in an aqueous solution containing 0.1 M K₃[Fe(CN)₆]-K₄[Fe(CN)₆] (1:1) and 0.1 M KCl using Zn₃In₂S₆/FTO as working electrodes. As shown in Fig. 13b, the resistance of the samples is determined by the radius of the arc at high frequencies on the EIS plots. As we know, the resistance value of

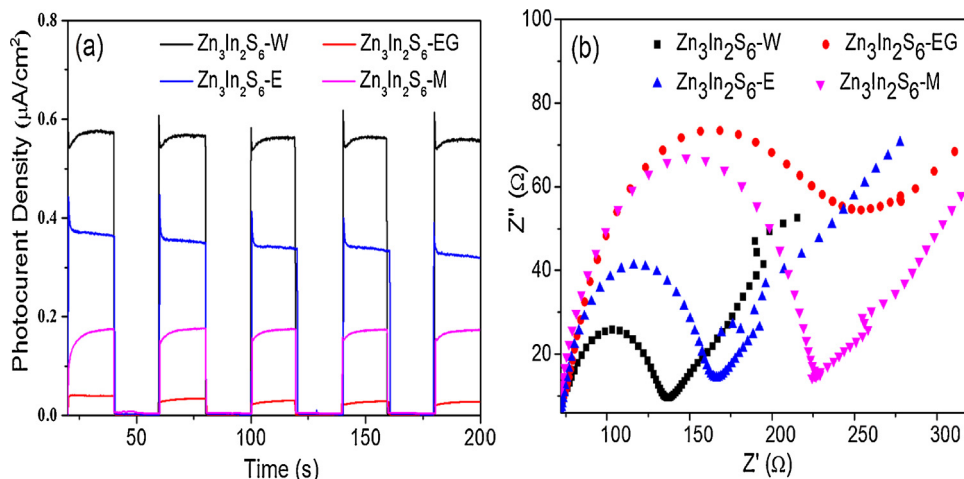


Fig. 13. Photocurrent density of $\text{Zn}_3\text{In}_2\text{S}_6$ sample electrodes in $0.2 \text{ M Na}_2\text{SO}_4$ solution without bias vs. Ag/AgCl under visible light irradiation (a). EIS Nyquist plots of the $\text{Zn}_3\text{In}_2\text{S}_6$ samples in an aqueous solution containing with $0.1 \text{ M K}_3[\text{Fe}(\text{CN})_6]\text{-K}_4[\text{Fe}(\text{CN})_6]$ (1:1) and 0.1 M KCl (b).

photocatalyst corresponds to radius of the arc in EIS Nyquist plots, and the smaller radius of the arcs it shows, the smaller resistance value it has. It can be observed from the figure that the EIS Nyquist plots of the $\text{Zn}_3\text{In}_2\text{S}_6\text{-W}$ sample has the smallest radius among the photocatalysts, reflecting that the conductive capability of $\text{Zn}_3\text{In}_2\text{S}_6\text{-W}$ sample is maximum, namely, the separation and transfer efficiency of photo-induced carriers for $\text{Zn}_3\text{In}_2\text{S}_6\text{-W}$ sample is the fastest. This result is consistent with the photocatalytic activities.

The Mott-Schottky experiments were conducted to evaluate the flat-band potential of the $\text{Zn}_3\text{In}_2\text{S}_6$ samples. It can be observed that the slope of the Mott-Schottky plot for all the samples is positive, suggesting the n-type characteristics of the as-synthesized semiconductors (Fig. S2). The flat band potential (E_{fb}) of semiconductor samples are calculated from the X intercepts of the linear region [20,30]. Thus the E_{fb} of $\text{Zn}_3\text{In}_2\text{S}_6$ samples are -0.48 , -0.61 , -0.58 and -0.50 V vs. Ag/AgCl for the different samples, respectively. Because the bottom of the CB is more negative by -0.1 V than the flat band potential for many n-type semiconductors and the converted potential of the NHE vs. Ag/AgCl is 0.2 V , the CB values of the samples are -0.38 , -0.51 , -0.48 and -0.40 eV vs. NHE for $\text{Zn}_3\text{In}_2\text{S}_6\text{-W}$, $\text{Zn}_3\text{In}_2\text{S}_6\text{-M}$, $\text{Zn}_3\text{In}_2\text{S}_6\text{-E}$ and $\text{Zn}_3\text{In}_2\text{S}_6\text{-EG}$ samples, respectively. Fig. 5 shows that the band gaps of $\text{Zn}_3\text{In}_2\text{S}_6$ are 2.81 , 2.62 , 2.81 and 2.52 eV for $\text{Zn}_3\text{In}_2\text{S}_6\text{-W}$, $\text{Zn}_3\text{In}_2\text{S}_6\text{-M}$, $\text{Zn}_3\text{In}_2\text{S}_6\text{-E}$ and $\text{Zn}_3\text{In}_2\text{S}_6\text{-EG}$ samples, respectively. Therefore, the corresponding VB potentials are 2.43 , 2.11 , 2.33 and 2.12 eV , respectively. In our previous report, the photocatalytic selective oxidation potential of benzyl alcohol to benzaldehyde is *ca.* $+0.68 \text{ V}$ (vs. NHE), and the reduction potential of hydrogen ions to hydrogen is *ca.* 0 V (vs. NHE) [22]. From Table 2, it can be found that the potentials of VB for $\text{Zn}_3\text{In}_2\text{S}_6$ samples are more positive than the oxidation potential for benzyl alcohol to benzaldehyde, and the potentials of the CB are more negative than the reduction potential for H^+ to H_2 . The above results show that the photocatalytic transformation of benzyl alcohol to benzaldehyde and H_2 evolution over $\text{Zn}_3\text{In}_2\text{S}_6$ samples can be achieved thermodynamically under light irradiation. This is consistent with our experimental results.

Table 2

The VB and CB values of $\text{Zn}_3\text{In}_2\text{S}_6$ samples obtained by DRS spectra and Mott-Schottky plots.

Samples	VB (eV)	CB (eV)	Band gap (eV)
$\text{Zn}_3\text{In}_2\text{S}_6\text{-W}$	2.43	-0.38	2.81
$\text{Zn}_3\text{In}_2\text{S}_6\text{-M}$	2.11	-0.51	2.62
$\text{Zn}_3\text{In}_2\text{S}_6\text{-E}$	2.33	-0.48	2.81
$\text{Zn}_3\text{In}_2\text{S}_6\text{-EG}$	2.12	-0.40	2.52

Additionally, the recombination rate of the photoinduced electron-hole pairs was examined by photoluminescence emission spectra (PL). As displayed in Fig.S3, the sequence of the PL intensity for the as-prepared samples is as follows: $\text{Zn}_3\text{In}_2\text{S}_6\text{-W} < \text{Zn}_3\text{In}_2\text{S}_6\text{-E} < \text{Zn}_3\text{In}_2\text{S}_6\text{-M} < \text{Zn}_3\text{In}_2\text{S}_6\text{-EG}$. Generally speaking, the stronger of the PL intensity corresponds to the greater recombination rate of the electron and hole pairs. Obviously, the $\text{Zn}_3\text{In}_2\text{S}_6\text{-W}$ has the weaker PL intensity than those of the other samples, reflecting its greater separation and transfer of photogenerated carrier. This result is consistent with the results of electrochemistry analysis. Moreover, the time-resolved photoluminescence (TRPL) decay spectra of $\text{Zn}_3\text{In}_2\text{S}_6$ samples were measured to study the recombination kinetics of photogenerated charge carriers. As shown in Fig. S4, the double exponential function ($I = A_1 e^{-t/\tau_1} + A_2 e^{-t/\tau_2} + A_3 e^{-t/\tau_3} + A_4 e^{-t/\tau_4}$) can be fitted based on the emission decay curves, and the results are shown in Table S1. Herein, the average charge carrier lifetime (τ) are estimated by the following equation [40,41]:

$$\tau = \frac{A_1 \tau_1^2 + A_2 \tau_2^2 + A_3 \tau_3^2 + A_4 \tau_4^2}{A_1 \tau_1 + A_2 \tau_2 + A_3 \tau_3 + A_4 \tau_4} \quad (6)$$

Thus, the calculated lifetimes of $\text{Zn}_3\text{In}_2\text{S}_6\text{-W}$, $\text{Zn}_3\text{In}_2\text{S}_6\text{-E}$, $\text{Zn}_3\text{In}_2\text{S}_6\text{-M}$ and $\text{Zn}_3\text{In}_2\text{S}_6\text{-EG}$ samples are 16.7 , 20.6 , 23.6 and 25.2 ns , respectively, suggesting that PL decay of $\text{Zn}_3\text{In}_2\text{S}_6\text{-W}$ is shorter than those of other photocatalysts. As we all know, the shorter PL decay can be beneficial for improving the photocatalytic performance, which is accordance with the previous reports [8,14].

3.3. Reaction mechanism

In order to study the effect of the photogenerated electrons and holes on the photocatalytic transformation of benzyl alcohol to benzaldehyde and H_2 evolution, a series of control experiments were carried out. Triethanolamine (TEA) and carbon tetrachloride (CCl_4) can be used as holes (h^+) and electrons(e^-) scavengers, respectively. As shown in Fig. 14a, when 1 mL CCl_4 is added into reaction system, the yields of benzaldehyde and hydrogen are 813.7 and $223.4 \mu\text{mol}$ under light irradiation for 4 h , respectively, which exhibits the yield of benzaldehyde is much greater than that of hydrogen. This is mainly because the electrons are removed after the addition of CCl_4 in the reaction system, and the amount of hydrogen evolution is greatly restrained. Accordingly, the oxidation of benzyl alcohol to benzaldehyde is accelerated by photogenerated holes. However, when 1 mL TEA is added into the reaction system, it can be observed from Fig. 14b that the yields of benzaldehyde and hydrogen are 57.5 and $111.1 \mu\text{mol}$ under light irradiation for 4 h , respectively, which suggest that the

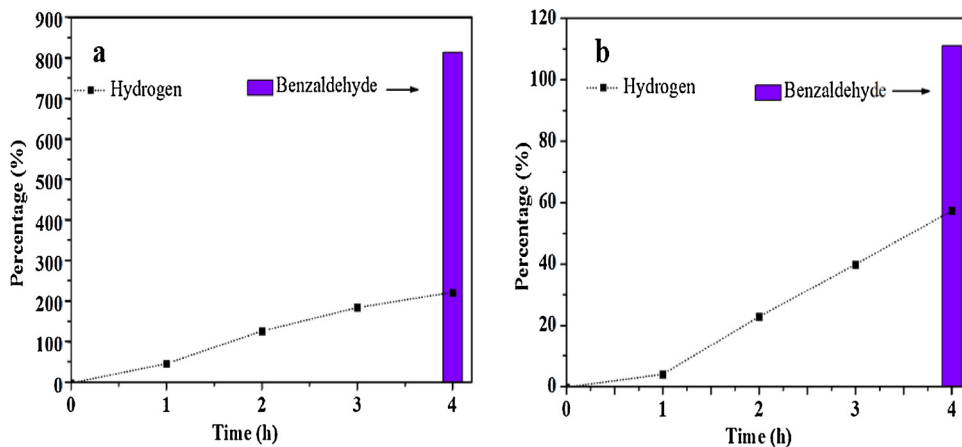


Fig. 14. Control experiments using different scavengers for photocatalytic transformation of benzyl alcohol to benzaldehyde and H₂ evolution over Zn₃In₂S₆-W sample under light irradiation for 4 h.

yields of benzaldehyde and H₂ evolution all decrease compared with the absence of TEA. This is mainly attribute to the decrease of the photogenerated holes with the addition of TEA, which hinders the photocatalytic dehydrogenation of benzyl alcohol to benzaldehyde and releasing H⁺, and further restricts the photocatalytic reduction of H⁺ to hydrogen by the photogenerated electrons. Based on the above analysis, it can be concluded that photogenerated h⁺ and e⁻ play significant roles in photocatalytic transformation of benzyl alcohol to benzaldehyde and H₂ evolution in this reaction system, and the photocatalytic oxidation of benzyl alcohol to benzaldehyde by the photogenerated holes is prior to the reduction of H⁺ to hydrogen by the photogenerated electrons.

The electron paramagnetic resonance (EPR) spin trapping technique is used to monitor the reaction intermediate in-situ. The characteristic EPR signals of the reaction system containing benzyl alcohol and Zn₃In₂S₆ samples under visible light irradiation ($\lambda > 420$ nm) are shown in Fig. 15. Six EPR peaks with the similar intensity in the Zn₃In₂S₆ photocatalysts are detected when DMPO (5,5-dimethyl-1-pyrrolineN-oxide) is added into the reaction system under visible light irradiation, which can be assigned to DMPO-carbon centered radical (DMPO-C) [12,27]. However, no signals can be detected in the dark or without photocatalyst, which confirms that it indeed goes through the photocatalytic transformation for aromatic alcohol to benzaldehyde and H₂ evolution. Moreover, the Zn₃In₂S₆-W sample has the strongest EPR intensity among the samples, corresponding to the more carbon-centered radicals formed in the system. Meanwhile, in our previous work, an isotopic tracing experiment using benzyl- α - α -d₂ alcohol (Ph-

CD₂OH) as a substrate was carried out. It has been demonstrated that the hydrogen protons come from α -H and hydroxyl hydrogen of benzyl alcohol, respectively. And the photocatalytic oxidation of benzyl alcohol to benzaldehyde by the photogenerated holes is prior to the photocatalytic reduction of H⁺ to hydrogen by the photogenerated electrons [20].

From the control experiments, it is demonstrated that the photogenerated electrons and holes play major roles for the photocatalytic transformation of benzyl alcohol to benzaldehyde and H₂ evolution. Coupled with the above analysis, a possible reaction mechanism for photocatalytic transformation of benzyl alcohol to benzaldehyde and H₂ evolution over Zn₃In₂S₆ sample under light irradiation is proposed (Scheme 1). The photogenerated electrons and holes are produced on the surface of Zn₃In₂S₆ sample under light illumination. The photogenerated holes in the VB position with a strong oxidation potential can oxidize benzyl alcohol to benzaldehyde, releasing two hydrogen

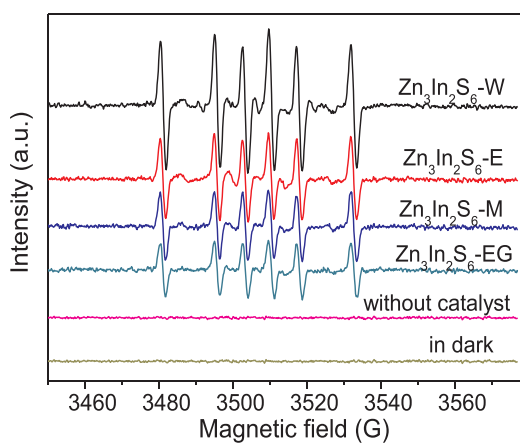
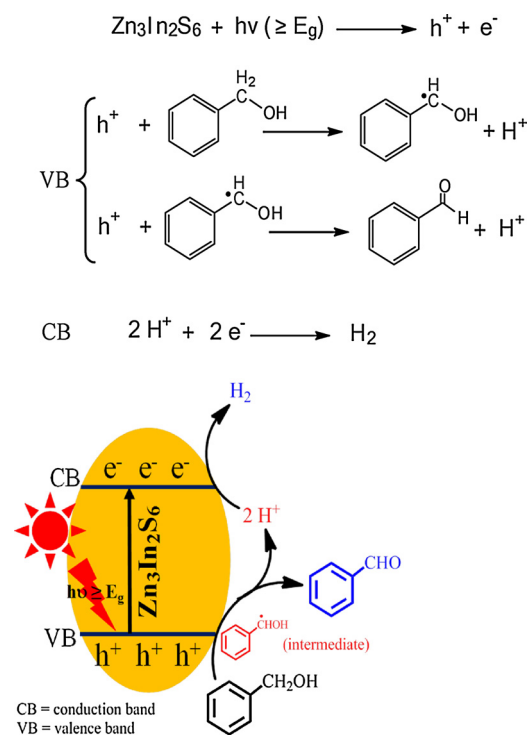


Fig. 15. EPR spectra of in-situ formed carbon-centered radicals in a reaction system of Zn₃In₂S₆ samples and benzyl alcohol.



Scheme 1. Proposed reaction mechanism of photocatalytic transformation of benzyl alcohol to benzaldehyde and H₂ evolution over Zn₃In₂S₆ sample under light irradiation.

protons (H^+). Subsequently, the released H^+ diffuses to the CB of photocatalyst and is reduced to H_2 by the photogenerated electrons. Because the diffusion process of H^+ has a certain lag property, the yield of benzaldehyde is slightly larger than that of hydrogen evolution.

4. Conclusion

In summary, $Zn_3In_2S_6$ samples were synthesized by a simple solvothermal method with different solvents. The $Zn_3In_2S_6$ -W exhibits an efficient photocatalytic activity and chemical stability. The photo-generated holes and electrons were effectively utilized for photocatalytic transformation of aromatic alcohols to aromatic aldehydes and H_2 evolution in a reaction system. In the reaction system, aromatic alcohols are oxidized to aromatic aldehydes and H^+ by the photo-excited holes, and the released H^+ is reduced to H_2 by the photo-generated electrons. The mole ratios between aromatic aldehydes and hydrogen are close to 1: 1. This paper not only constructs a system for effective utilization of photogenerated electrons and holes for aromatic alcohol to aromatic aldehydes and hydrogen evolution, but also provides a new reaction system for nitrogen fixation and CO_2 reduction.

Acknowledgements

This work was financially supported by the Natural Science Foundation of China (NSFC, grant Nos. 51472005, 21603002 and 51772118), the Natural Science Foundation of Anhui province (Grant Nos. 1608085QB37 and 1808085QE141), the Outstanding Youth Foundation of Anhui Province (No. 1808085J24), the Open Foundation of Nano-mineral materials and application of the Ministry of Education Engineering Research Center (NGM2018KF006), and the Materials Science and Engineering Key Discipline Foundation (No. AKZDXK2015A01).

Appendix A. Supplementary data

Supplementary material related to this article can be found, in the online version, at doi:<https://doi.org/10.1016/j.apcatb.2018.10.004>.

References

- [1] J. Liu, Y. Liu, N. Liu, Y. Han, X. Zhang, H. Huang, Y. Lifshitz, S. Lee, J. Zhong, Z. Kang, *Science* 347 (2015) 970–974.
- [2] Y. Zheng, L. Lin, X. Ye, F. Guo, X. Wang, *Angew. Chem. Int. Ed.* 53 (2014) 1–6.
- [3] Y. Wang, H. Wang, F. Chen, F. Cao, X. Zhao, S. Meng, Y. Cui, *Appl. Catal. B: Environ.* 206 (2017) 417–425.
- [4] A. Fujishima, K. Honda, *Nature* 238 (1972) 37–38.
- [5] A. Weingarten, R. Kazantsev, L. Palmer, D. Fairfield, A. Koltonow, S. Stupp, *J. Am. Chem. Soc.* 137 (2015) 15241–15246.
- [6] D. Kim, D. Whang, S. Park, *J. Am. Chem. Soc.* 138 (2016) 8698–8701.
- [7] T. Stoll, M. Gennari, J. Fortage, C. Castillo, M. Rebarz, M. Sliwa, O. Poizat, F. dobé, A. Deronzier, M. Collomb, *Angew. Chem. Int. Ed.* 53 (2014) 1654–1658.
- [8] X. Wang, K. Maeda, X. Chen, K. Takanabe, K. Domen, Y. Hou, X. Fu, M. Antonietti, *J. Am. Chem. Soc.* 131 (2009) 1680–1681.
- [9] X. Zong, H. Yan, G. Wu, G. Ma, F. Wen, L. Wang, C. Li, *J. Am. Chem. Soc.* 130 (2008) 7176–7177.
- [10] Y. Su, Z. Zhang, H. Liu, Y. Wang, *Appl. Catal. B: Environ.* 200 (2017) 448–457.
- [11] X. Wang, K. Maeda, A. Thomas, K. Takanabe, G. Xin, J. Carlsson, K. Domen, M. Antonietti, *Nat. Mater.* 8 (2009) 76–80.
- [12] D. Jiang, X. Chen, Z. Zhang, L. Zhang, Y. Wang, Z. Sun, R. Irfan, P. Du, *J. Catal.* 357 (2018) 147–153.
- [13] X. Fu, L. Zhang, L. Liu, H. Li, S. Meng, X. Ye, S. Chen, *J. Mater. Chem. A* 5 (2017) 15287–15293.
- [14] X. Chen, Y. Jun, K. Takanabe, K. Maeda, K. Domen, X. Fu, M. Antonietti, X. Wang, *Chem. Mater.* 21 (2009) 4093–4095.
- [15] J. Ran, W. Guo, H. Wang, B. Zhu, J. Yu, S. Qiao, *Adv. Mater.* (2018), <https://doi.org/10.1002/adma.201800128>.
- [16] Y. Hou, A. Laursen, J. Zhang, G. Zhang, Y. Zhu, X. Wang, S. Dahl, I. Chorkendorff, *Angew. Chem. Int. Ed.* 52 (2013) 1–6.
- [17] J. Zhang, M. Zhang, R. Sun, X. Wang, *Angew. Chem. Int. Ed.* 51 (2012) 10145–10149.
- [18] Q. Xiao, Z. Liu, A. Bo, S. Zavahir, S. Sarina, S. Bottle, J. Riches, H. Zhu, *J. Am. Chem. Soc.* 137 (2015) 1956–1966.
- [19] B. Zope, D. Hibbitts, M. Neurock, R. Davis, *Science* 330 (2010) 74–78.
- [20] C. Ling, X. Ye, J. Zhang, J. Zhang, S. Zhang, S. Meng, X. Fu, S. Chen, *Sci. Rep.* 7 (2017) 27.
- [21] S. Meng, X. Ye, X. Ning, M. Xie, X. Fu, S. Chen, *Appl. Catal. B: Environ.* 182 (2016) 356–368.
- [22] X. Ning, S. Meng, X. Fu, X. Ye, S. Chen, *Green Chem.* 18 (2016) 3286–3369.
- [23] L. Su, X. Ye, S. Meng, X. Fu, S. Chen, *Appl. Surf. Sci.* 384 (2016) 161–174.
- [24] M. Xie, X. Dai, S. Meng, X. Fu, S. Chen, *Chem. Eng. J.* 245 (2014) 107–116.
- [25] X. Dai, M. Xie, S. Meng, X. Fu, S. Chen, *Appl. Catal. B: Environ.* 158–159 (2014) 382–390.
- [26] J. Zhang, S. Meng, X. Ye, C. Ling, S. Zhang, X. Fu, S. Chen, *Appl. Catal. B: Environ.* 218 (2017) 420–429.
- [27] H. Li, F. Qin, Z. Yang, X. Cui, J. Wang, L. Zhang, *J. Am. Chem. Soc.* 139 (2017) 3513–3521.
- [28] W. Song, A. Vannucci, B. Farnum, A. Lapides, M. Brennaman, B. Kalanyan, L. Alibabaei, J. Concepcion, M. Losego, G. Parsons, T. Meyer, *J. Am. Chem. Soc.* 136 (2014) 9773–9779.
- [29] X. Ye, Y. Chen, C. Ling, J. Zhang, S. Meng, X. Fu, X. Wang, S. Chen, *Chem. Engin. J.* 348 (2018) 966–977.
- [30] Y. Wu, X. Ye, S. Zhang, S. Meng, X. Fu, X. Wang, X. Zhang, S. Chen, *J. Catal.* 359 (2018) 151–160.
- [31] S. Shen, L. Zhao, L. Guo, *Int. J. Hydrogen Energy* 35 (2010) 10148–10154.
- [32] L. Ye, J. Fu, Z. Xu, R. Yuan, Z. Li, *ACS Appl. Mater. Interfaces* 6 (2014) 3483–3490.
- [33] L. Ye, Z. Li, *ChemCatChem* 6 (2014) 2540–2543.
- [34] L. Yuan, M. Yang, Y. Xu, *J. Mater. Chem. A* 2 (2014) 14401–14412.
- [35] J. Chen, H. Zhang, P. Liu, Y. Li, X. Liu, G. Li, P. Wong, T. An, H. Zhao, *Appl. Catal. B: Environ.* 168–169 (2015) 266–273.
- [36] B. Xu, P. He, H. Liu, P. Wang, G. Zhou, X. Wang, *Angew. Chem. Int. Ed.* 53 (2014) 2339–2343.
- [37] L. Ye, Z. Li, *Appl. Catal. B: Environ.* 160–161 (2014) 552–557.
- [38] X. Ye, Y. Cui, X. Qiu, X. Wang, *Appl. Catal. B: Environ.* 152–153 (2014) 383–389.
- [39] S. Chen, Y. Hu, S. Meng, X. Fu, *Appl. Catal. B: Environ.* 150–151 (2014) 564–573.
- [40] D. Xu, B. Cheng, W. Wang, C. Jiang, J. Yu, *Appl. Catal. B: Environ.* 231 (2018) 368–380.
- [41] J. Wang, Y. Xia, H. Zhao, G. Wang, L. Xiang, J. Xu, S. Komarneni, *Appl. Catal. B: Environ.* 206 (2017) 406–416.